QUARTERLY OF APPLIED MATHEMATICS
VOLUME LVI, NUMBER 2
JUNE 1998, PAGES 221–244

DYNAMICS OF A VISCOELASTIC SPHERICAL SHELL WITH A NONCONVEX STRAIN ENERGY FUNCTION

BY

ROGER FOSDICK, YOHANNES KETEMA, AND JANG-HORNG YU

Department of Aerospace Engineering and Mechanics, University of Minnesota, Minneapolis, Minnesota

Abstract. We study the radial motion of an incompressible viscoelastic spherical shell with a nonconvex strain energy function that models a material that can undergo a phase transition. In addition to the classical *Newtonian* viscosity for viscoelastic materials, we consider a material with two microstructural coefficients that are supposed to sense local configurational changes that take place during a deformation. Conditions necessary to show the effect of the nonconvexity of the strain energy function during a phase transition of the material, are determined, and the resulting dynamics is analyzed. It is shown that, though small periodic vibrations are possible, the system can easily revert into a mode of large amplitude motion as a result of small external excitation. Such motion may be transient to periodic motion or to chaotic motion. Boundaries in parameter space for the occurrence of this type of motion are determined and examples are given.

1. Introduction. The phenomenon of phase transition in the development of devices and so-called "smart materials" has drawn considerable interest in both fundamental studies and practical applications. For example, shape memory alloys are used extensively in the field of active vibration control to serve as sensors, actuators, and structural components in vibrational structures. Therefore, a fundamental understanding of the dynamical characteristics of these types of materials is essential.

The purpose of this study is to investigate the effects of viscoelasticity on the dynamical behavior of materials that exhibit pseudoelastic behavior and hysteresis. Pseudoelastic behavior often involves a diffusionless phase transition for which there is a resultant change in the material microstructure due to the austenitic-to-martensitic transformation. Falk [7], Abeyaratne and Knowles [1], and Leo, Shield and Bruno [16] have given insight as to how a nonconvex elastic free energy function might appropriately describe this behavior. On the other hand, to consider what part the microstructural changes could play in the dynamical behavior of viscoelastic materials, Fosdick, Warner and Yu [9] included non-Newtonian second-grade terms in the constitutive model and studied the

Received March 21, 1995.
1991 *Mathematics Subject Classification.* Primary 70K05, 70K10, 70K40, 73B99, 73D35, 73F15, 73G25, 73H10, 73K12, 73K15, 73K50.

structure of steady shock waves. In this model the non-Newtonian effects were attributed to the local microstructural configurational changes that the material would experience during the deformation.

The modelling of shape memory materials by the use of a nonconvex strain energy function is still a controversial subject, but experiments are beginning to suggest that nonconvexities are a plausible part of the story. We therefore hope that the distinct dynamical characteristics that are predicted in this work will prove to be a useful basis for experiments in the study of these materials.

We shall consider the radial motion of a spherical shell in order to be specific and detailed about the dynamical behavior: the material is viscoelastic with a nonconvex strain energy function. There are a few studies concerning the classical vibration of viscoelastic spherical shells, but they do not deal with such things as nonconvexities and the possibility of chaotic motion. For example, Gautham and Ganesan [10] have investigated the damping characteristics of an elastic spherical shell with a viscoelastic core, and there have been related works [17], [5] on spherical shells containing viscoelastic layers.

We begin in Sec. 2 by introducing the constitutive model of an incompressible second-grade solid whose viscoelasticity is characterized by two microstructural coefficients α_1 and α_2 in addition to the classical Newtonian viscosity. By restricting the motion to be radial and invoking the balance of linear momentum, we arrive at the specific dynamical system as recorded in Sec. 3.

In Sec. 4 we rewrite the dynamical system in canonical Hamiltonian form temporarily disregarding the viscosity and external forcing. Then, in Sec. 5, we use a number of known results on the behavior of such reduced systems in order to establish a basis for our study of the full system. We find that the microstuctural coefficients enter the system as a dynamical potential which is proportional to the square of the generalized momentum—they have no effect on the location of equilibrium points but they do have an effect on their stability. The nonconvexity of the strain energy function manifests itself with a double well potential in the region of phase transition. The bifurcations that lead to both the creation and depletion of this double well structure are explained.

In Sec. 6, we study the effects of small-viscosity and small time-periodic forcing. Melnikov's method is used to determine the occurrence and stability of small-amplitude orbits not only about an equilibrium point while remaining in a single phase, but also about both equilibrium points *during* the process of phase transition. It is shown that stable steady state behavior consisting of a simple small-amplitude oscillation about a fixed point is not always the result of small time-periodic forcing programs: large-amplitude chaotic transients can occur due to the formation of homoclinic orbits. Conditions for the existence of such chaotic transients also are determined by using a form of Melnikov's method.

2. Constitutive assumptions. We shall consider a constitutive structure that corresponds to an incompressible, isotropic solid of second grade. Thus, the material is expected to exhibit both elastic response and mechanical dissipation effects as it is deformed. Our basic assumption is that the Cauchy stress $\mathbf{T}$ can be represented as the

sum of an elastic and constraint reaction part

$$\mathbf{T}^e = -p\mathbf{1} + \widehat{\mathbf{T}}^e(\mathbf{F}), \tag{1}$$

where $\widehat{\mathbf{T}}^e$ is a symmetric tensor-valued function of the deformation gradient $\mathbf{F}$, and a dissipative part

$$\mathbf{T}^d = \mu\mathbf{A}_1 + \alpha_1\mathbf{A}_2 + \alpha_2\mathbf{A}_1^2, \tag{2}$$

where $\mathbf{A}_1$ and $\mathbf{A}_2$ are the first two *Rivlin-Ericksen* tensors,

$$\mathbf{A}_1 = \mathbf{L} + \mathbf{L}^{\mathrm{T}} \tag{3}$$

and

$$\mathbf{A}_2 = \dot{\mathbf{A}}_1 + \mathbf{A}_1\mathbf{L} + \mathbf{L}^{\mathrm{T}}\mathbf{A}_1. \tag{4}$$

Here, $\mathbf{L}$ represents the spatial velocity gradient, a superposed dot denotes the material time derivative, μ is the classical Newtonian viscosity, and the coefficients α_1 and α_2 represent the effect that the local geometric microstructure of the body has on its viscoelastic response [9]. Thus, we take

$$\mathbf{T} = \mathbf{T}^e + \mathbf{T}^d = -p\mathbf{1} + \widehat{\mathbf{T}}^e(\mathbf{F}) + \mu\mathbf{A}_1 + \alpha_1\mathbf{A}_2 + \alpha_2\mathbf{A}_1^2. \tag{5}$$

Since the material is incompressible, then any motion $\mathbf{x} = \chi(\mathbf{X}, t)$ must be isochoric so that $\det \nabla\chi = 1$. As is common, we let $\mathbf{X}$ denote the reference point of a material particle, $\mathbf{x}$ its present position, t the time, and $\mathbf{F} = \nabla\chi$ the deformation gradient introduced earlier. Clearly, the chain rule requires $\dot{\mathbf{F}} = \mathbf{L}\mathbf{F}$.

Because of incompressibility, the constraint reaction part of the stress, $-p\mathbf{1}$, is arbitrary and non-constitutive. Moreover, because of isotropy, we may, without loss of generality, replace $\widehat{\mathbf{T}}^e(\mathbf{F})$ by the form

$$\widehat{\mathbf{T}}^e(\mathbf{F}) = \beta_1\mathbf{B} + \beta_{-1}\mathbf{B}^{-1}, \tag{6}$$

where $\mathbf{B} = \mathbf{F}\mathbf{F}^{\mathrm{T}}$ is the left Cauchy-Green strain tensor, and β_1 and β_{-1} are functions of the invariants $I_{\mathbf{B}} = \operatorname{tr}\mathbf{B}$ and $I_{\mathbf{B}^{-1}} = \operatorname{tr}\mathbf{B}^{-1}$. These are determined in terms of the volumetric strain energy function $W(I_{\mathbf{B}}, I_{\mathbf{B}^{-1}})$ through

$$\begin{aligned} \beta_1(I_{\mathbf{B}}, I_{\mathbf{B}^{-1}}) &= 2\frac{\partial W(I_{\mathbf{B}}, I_{\mathbf{B}^{-1}})}{\partial I_{\mathbf{B}}}, \\ \beta_{-1}(I_{\mathbf{B}}, I_{\mathbf{B}^{-1}}) &= -2\frac{\partial W(I_{\mathbf{B}}, I_{\mathbf{B}^{-1}})}{\partial I_{\mathbf{B}^{-1}}}. \end{aligned} \tag{7}$$

In Sec. 4, we shall consider the strain energy function W to be a source of nonconvexity so as to study the effect that a potential phase transformation has on the dynamics of an oscillating spherical shell. In recent years, the introduction of a nonconvex stored energy function has been an important element in the investigation of materials that exhibit phase transition phenomena such as shape memory alloys.[1]

Combining (5) and (6), we obtain the form of the constitutive assumption that we shall adopt for the Cauchy stress. In addition, we shall assume that this form satisfies the thermodynamical requirements [20] that $\mu \geq 0$, $\alpha_1 + \alpha_2 = 0$, and $\alpha_1 \geq 0$.

[1]See, for example, Falk [7] or Abeyaratne and Knowles [1].

3. Kinematics and dynamical equation. Here, we develop the dynamical equation that governs the radial motion of a hollow spherical shell. Let $\mathbf{X} = \{R, \Theta, \Phi\}$ and $\mathbf{x} = \{r, \theta, \varphi\}$ denote the referential and current spherical coordinates of the particles of a spherical shell, respectively. In the reference configuration the inner and outer radii are a_0 and b_0, respectively, and the shell is subject to an internal pressure $P_1(t)$ and an external pressure $P_2(t)$. Since the motion is restricted to be radial, we may express it according to

$$\begin{cases} r = f(R,t), \\ \theta = \Theta, \\ \varphi = \Phi. \end{cases} \tag{8}$$

Thus, relative to an orthonormal spherical base, the deformation gradient has the form

$$\mathbf{F}(t) = \begin{bmatrix} \frac{\partial f}{\partial R} & 0 & 0 \\ 0 & \frac{f}{R} & 0 \\ 0 & 0 & \frac{f}{R} \end{bmatrix},$$

and the incompressibility condition, $\det \mathbf{F}(t) = 1$, requires that

$$\frac{\partial f}{\partial R}\left(\frac{f}{R}\right)^2 = 1.$$

Therefore,

$$r^3(t) = [f(R,t)]^3 = R^3 + \nu(t). \tag{9}$$

If the current inner and outer radii are denoted by $a(t)$ and $b(t)$, respectively, then

$$\nu(t) = a^3(t) - a_0^3 = b^3(t) - b_0^3, \tag{10}$$

and, since (10) describes the motion of the whole spherical shell, we only need to focus on the motion of the inner radius $a(t)$.

The left Cauchy-Green strain tensor and its inverse are

$$\mathbf{B}(t) = \begin{bmatrix} \frac{R^4}{r^4} & 0 & 0 \\ 0 & \frac{r^2}{R^2} & 0 \\ 0 & 0 & \frac{r^2}{R^2} \end{bmatrix} \tag{11}$$

and

$$\mathbf{B}^{-1}(t) = \begin{bmatrix} \frac{r^4}{R^4} & 0 & 0 \\ 0 & \frac{R^2}{r^2} & 0 \\ 0 & 0 & \frac{R^2}{r^2} \end{bmatrix}. \tag{12}$$

In addition, the first and second Rivlin-Ericksen tensors defined in (3), (4) can readily be shown to have the form

$$\mathbf{A}_1(t) = \begin{bmatrix} -\frac{4}{3}\frac{\dot{\nu}(t)}{r^3} & 0 & 0 \\ 0 & \frac{2}{3}\frac{\dot{\nu}(t)}{r^3} & 0 \\ 0 & 0 & 0 \end{bmatrix} \tag{13}$$

and

$$\mathbf{A}_2(t) = \begin{bmatrix} -\frac{4}{3}\frac{\ddot{\nu}(t)}{r^3} + \frac{28}{9}\frac{\dot{\nu}(t)^2}{r^6} & 0 & 0 \\ 0 & \frac{2}{3}\frac{\ddot{\nu}(t)}{r^3} - \frac{2}{9}\frac{\dot{\nu}(t)^2}{r^6} & 0 \\ 0 & 0 & 0 \end{bmatrix}. \tag{14}$$

The balance of linear momentum, without body force, has the form

$$\operatorname{div} \mathbf{T} = \rho \mathbf{a}, \tag{15}$$

where ρ is the constant mass density and $\mathbf{a}$ is the acceleration. Thus, with the constitutive structure (5), (6), and the restriction to radial motion, (15) may be reduced to the following scalar equations:

$$\begin{cases} \frac{\partial T_{rr}}{\partial r} + \frac{2}{r}(T_{rr} - T_{\theta\theta}) = \rho \ddot{r}, \\ \frac{\partial T_{\theta\theta}}{\partial \theta} = 0, \\ \frac{\partial T_{\varphi\varphi}}{\partial \varphi} = 0. \end{cases} \tag{16}$$

It is well known [18] that the acceleration for this motion may be expressed as

$$\ddot{r} = \frac{\partial \zeta}{\partial r}, \tag{17}$$

where

$$\zeta = \frac{1}{3r}\left(-\ddot{\nu} + \frac{1}{6}\frac{\dot{\nu}^2}{r^3}\right). \tag{18}$$

Now, by substituting (11), (12), (13), and (14) into (5) and (6) in order to explicitly calculate the stress terms in (16), and by using (17), (18), we see that (16) is a restriction on the two unknown fields $a(t)$ (or $\nu(t)$) and $p(\mathbf{x}, t)$. To satisfy the second and third equations of (16), we find that $p = p(r, t)$, and by integrating the first of (16) and using the pressure boundary conditions on the inner and outer walls of the shell, we determine $p(r, t)$ in terms of $a(t)$—in addition, after some simplification we arrive at[2] the differential equation

$$\begin{aligned} &x\ddot{x}\left[1 - \left(1 + \frac{\Delta}{x^3}\right)^{-\frac{1}{3}}\right] + \dot{x}^2\left[\frac{3}{2} - 2\left(1 + \frac{\Delta}{x^3}\right)^{-\frac{1}{3}} + \frac{1}{2}\left(1 + \frac{\Delta}{x^3}\right)^{-\frac{4}{3}}\right] + g(x;\Delta) \\ &+ \frac{1}{\rho a_0^2}\left\{\frac{4\mu\Delta\dot{x}}{x(x^3+\Delta)} - \frac{(10\alpha_1 + 4\alpha_2)\Delta(2x^3+\Delta)\dot{x}^2}{x^2(x^3+\Delta)^2} + \frac{8\alpha_1\Delta\dot{x}^2}{x^2(x^3+\Delta)} + \frac{4\alpha_1\Delta\ddot{x}}{x(x^3+\Delta)}\right\} = \frac{P(t)}{\rho a_0^2}. \end{aligned} \tag{19}$$

Here, we have introduced the normalized quantities

$$x(t) \equiv \frac{a(t)}{a_0} > 0, \qquad \Delta \equiv \frac{b_0^3}{a_0^3} - 1 > 0, \qquad P(t) \equiv P_1(t) - P_2(t), \tag{20}$$

as well as the residual elastic response function

$$g(x;\Delta) = \frac{2}{3\rho a_0^2}\int_{\frac{x^3+\Delta}{\Delta+1}}^{x^3} u^{-\frac{7}{3}}(1+u)\Lambda(u)\,du. \tag{21}$$

[2]See [19] for details.

The function $\Lambda(u)$ in (21) is determined from the elastic response functions $\beta_1(I_{\mathbf{B}}, I_{\mathbf{B}^{-1}})$ and $\beta_{-1}(I_{\mathbf{B}}, I_{\mathbf{B}^{-1}})$ and has the form

$$\Lambda(u) = \beta_1(I_{\mathbf{B}}, I_{\mathbf{B}^{-1}}) - u^{\frac{2}{3}}\beta_{-1}(I_{\mathbf{B}}, I_{\mathbf{B}^{-1}}), \tag{22}$$

where the substitution variable $u = R^3/r^3$ and, according to (11), (12),

$$I_{\mathbf{B}} = u^{\frac{4}{3}} + 2u^{-\frac{2}{3}}, \qquad I_{\mathbf{B}^{-1}} = u^{-\frac{4}{3}} + 2u^{\frac{2}{3}}. \tag{23}$$

We note that the *Baker-Ericksen* inequality (see [2] or [8]) requires $\Lambda(u) \geq 0$, which we shall adopt. Because it will be convenient later to have available a dimensionless form of the elastic material function $\Lambda(u)$, we introduce

$$\overline{\Lambda}(u) = \frac{\Lambda(u)}{\Lambda_0}, \tag{24}$$

where Λ_0 is a fixed normalization of $\Lambda(u)$ having the dimension of force/(length)^2.

When the thermodynamic requirement $\alpha_1 + \alpha_2 = 0$ from [20] is substituted into (19) we get

$$\begin{aligned} &x\ddot{x}\left[1 - \left(1 + \frac{\Delta}{x^3}\right)^{-\frac{1}{3}}\right] + \dot{x}^2\left[\frac{3}{2} - 2\left(1 + \frac{\Delta}{x^3}\right)^{-\frac{1}{3}} + \frac{1}{2}\left(1 + \frac{\Delta}{x^3}\right)^{-\frac{4}{3}}\right] + g(x;\Delta) \\ &+ \frac{1}{\rho a_0^2}\left\{\frac{4\mu\Delta\dot{x}}{x(x^3+\Delta)} - \frac{6\alpha_1\Delta(2x^3+\Delta)\dot{x}^2}{x^2(x^3+\Delta)^2} + \frac{8\alpha_1\Delta\dot{x}^2}{x^2(x^3+\Delta)} + \frac{4\alpha_1\Delta\ddot{x}}{x(x^3+\Delta)}\right\} = \frac{P(t)}{\rho a_0^2}, \end{aligned} \tag{25}$$

which may be put into dimensionless form by introducing the parameter $\Omega > 0$ according to

$$\frac{\Lambda_0}{\rho a_0^2 \Omega^2} = 1. \tag{26}$$

Because Ω has the dimension of reciprocal time, we define the dimensionless time τ through

$$\tau = \Omega t, \tag{27}$$

and then by redefining the superposed dot so that it represents a derivative with respect to τ, we find that (25) becomes

$$\begin{aligned} &x\ddot{x}\left[1 - \left(1 + \frac{\Delta}{x^3}\right)^{-\frac{1}{3}}\right] + \dot{x}^2\left[\frac{3}{2} - 2\left(1 + \frac{\Delta}{x^3}\right)^{-\frac{1}{3}} + \frac{1}{2}\left(1 + \frac{\Delta}{x^3}\right)^{-\frac{4}{3}}\right] + \overline{g}(x;\Delta) \\ &+ \varepsilon\overline{\mu}\frac{4\Delta\dot{x}}{x(x^3+\Delta)} + \overline{\alpha}\left\{-\frac{6\Delta(2x^3+\Delta)\dot{x}^2}{x^2(x^3+\Delta)^2} + \frac{8\Delta\dot{x}^2}{x^2(x^3+\Delta)} + \frac{4\Delta\ddot{x}}{x(x^3+\Delta)}\right\} = \overline{P}(\tau), \end{aligned} \tag{28}$$

where

$$\varepsilon\overline{\mu} = \frac{\mu}{\sqrt{\rho a_0^2 \Lambda_0}}, \tag{29}$$

$$\overline{\alpha} = \frac{\alpha_1}{\rho a_0^2}, \tag{30}$$

$$\overline{g}(x;\Delta) = \frac{g(x;\Delta)\rho a_0^2}{\Lambda_0}, \tag{31}$$

and

$$\overline{P}(\tau) = \frac{P(t)}{\Lambda_0}. \tag{32}$$

Later in this work, we will assume that the viscosity is small, so that $\varepsilon \ll 1$, and consider this case as a perturbation from the situation when $\varepsilon = 0$.

4. Canonical formulation. Having introduced the dimensionless time τ above, throughout the remainder of this work we shall identify the symbol τ with t and henceforth let t represent the dimensionless time variable. Also, we assume that

$$\overline{P}(t) = P_0 + \varepsilon f \sin(\omega t), \tag{33}$$

where $P_0 \geq 0$ is constant, $0 \leq \varepsilon \ll 1$ and $f \geq 0$. We can then write (28) in the form

$$\frac{d}{dt}\left(\frac{\partial \mathcal{L}}{\partial \dot{x}}\right) - \frac{d\mathcal{L}}{dx} = x^2 \varepsilon f \sin(\omega t) - \frac{4\varepsilon \overline{\mu} \Delta \dot{x}}{x(x^3 + \Delta)}, \tag{34}$$

where

$$\mathcal{L} = T - \mathcal{W} = \mathcal{L}(x, \dot{x}) \tag{35}$$

is the Lagrangian function which is defined in terms of the (dimensionless) kinetic energy

$$T = T(x, \dot{x}) = \frac{1}{2} x^3 \dot{x}^2 \left(1 - \left(1 + \frac{\Delta}{x^3}\right)^{\frac{1}{3}}\right), \tag{36}$$

and the potential energy

$$\mathcal{W} = \mathcal{W}(x, \dot{x}) = G(x; \Delta) - \frac{1}{2} \frac{4\overline{\alpha} \Delta x}{(x^3 + \Delta)} \dot{x}^2 - P_0 \frac{x^3}{3}. \tag{37}$$

Notice that the potential energy includes a dynamical term proportional to $\dot{x}^2$, and that the function

$$G(x; \Delta) = \int_1^x \overline{g}(y; \Delta) y^2 \, dy, \tag{38}$$

because of (21), (22), and (31), is associated with the elasticity of the shell. To be definite, we shall consider a nonconvex elastic energy function $G(x; \Delta)$ in (38) such that $\overline{g}(x; \Delta)$ of (21), (22), (23), (24), and (31) has the form

$$\overline{g}(x; \Delta) = \frac{2}{3} \int_{\frac{x^3 + \Delta}{\Delta + 1}}^{x^3} u^{-\frac{7}{3}} (1 + u) \overline{\Lambda}(u) \, du$$

with

$$\overline{\Lambda}(u) = 0.15(u^{\frac{4}{3}} + 2u^{-\frac{2}{3}})^2 - 1.95(u^{\frac{4}{3}} + 2u^{-\frac{2}{3}}) + 9. \tag{39}$$

The form of (39) is not based on experimental data, and is chosen only as an example for this work.

In the remainder of this work we shall use canonical variables since this will enable us to more directly make use of numerous results on the dynamics of Hamiltonian systems and perturbations of such systems for small ε. Thus, to obtain the basic Hamiltonian system that corresponds to (34) we temporarily set $\varepsilon = 0$ and defer until later the consideration of small forcing and viscosity.

Let the generalized coordinate q be defined by

$$q = x. \tag{40}$$

Then, we have $\mathcal{L} = \mathcal{L}(q, \dot{q})$, and the generalized momentum p is defined according to

$$p = \frac{\partial \mathcal{L}(q, \dot{q})}{\partial \dot{q}}. \tag{41}$$

Because of (35), (36), and (37), p has the explicit form

$$p = Q(q)\dot{q}, \tag{42}$$

where

$$Q(q) = q^3 \left(1 - \left(1 + \frac{\Delta}{q^3}\right)^{\frac{1}{3}}\right) + \frac{4\overline{\alpha}\Delta q}{(q^3 + \Delta)}. \tag{43}$$

Now, for the Hamiltonian of the system we find that

$$H(q, p) = [\dot{q}p - \mathcal{L}(q, \dot{q})]_{\dot{q} = \frac{p}{Q(q)}} = \frac{p^2}{2Q(q)} + V(q; \Delta), \tag{44}$$

where

$$V(q; \Delta) = G(q; \Delta) - P_0 \frac{q^3}{3}. \tag{45}$$

A simple verification shows that q and p are in fact canonical variables, and that $H(q, p)$ defined in (44) is the corresponding Hamiltonian so that

$$\dot{q} = \frac{\partial H}{\partial p} = \frac{p}{Q(q)}, \tag{46}$$

$$\dot{p} = -\frac{\partial H}{\partial q} = \frac{p^2 Q'(q)}{2Q(q)^2} - V'(q; \Delta), \tag{47}$$

where the prime on $V(q; \Delta)$ denotes differentiation with respect to q. Of course, on any trajectory $(q, p)(t)$ of this system, $H(q(t), p(t))$ is constant.

5. Free oscillations. Let us now set $\varepsilon = 0$ and consider the case of undamped free oscillations. The dynamical equations are given by (46) and (47), and the parameters of interest are $\overline{\alpha}, P_0$, and Δ.

For $P_0 = 0$, (46) and (47) have one equilibrium point at $(q, p) = (0, 1)$ for all values of Δ. In this case the equilibrium value of q must be a zero of the function $\overline{g}(q; \Delta)$ of (39), as can be seen by using the definition of $V(q; \Delta)$ from (45) and (38) in (47). The dependence of the function $\overline{g}(q; \Delta)$ on Δ is illustrated in Fig. 1. Clearly as Δ is increased $\overline{g}(\cdot; \Delta)$ changes from a nonmonotone function into a strictly decreasing function.

Figure 2 shows the phase portrait, i.e., the level curves $H(q, p) = const.$, of this system for the case $P_0 = 0, \overline{\alpha} = 0$, and $\Delta = 1$. The system has one elliptic equilibrium point (i.e., the Hessian of $H(q, p)$ has purely imaginary eigenvalues) at $(q, p) = (1, 0)$. Figure 3 (see p. 230) shows the cross section $H = H(q, 0) = V(q; 1)$ for this situation. Clearly, $H = H(q, p)$ represents a single-well potential.

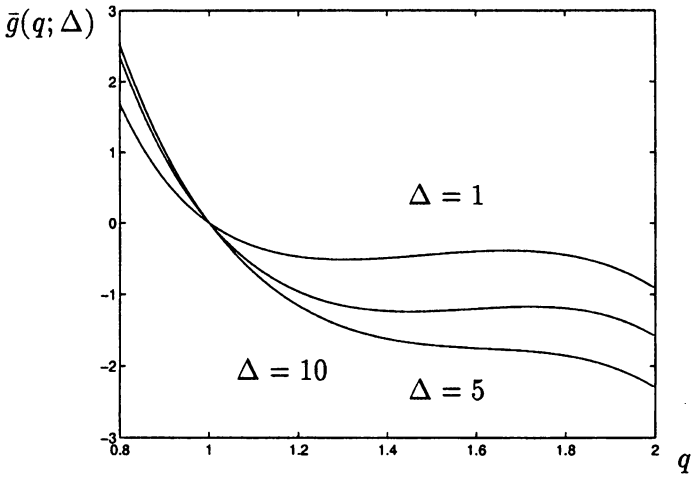

FIG. 1. The effect of changing Δ on the function $\bar{g}(q;\Delta)$

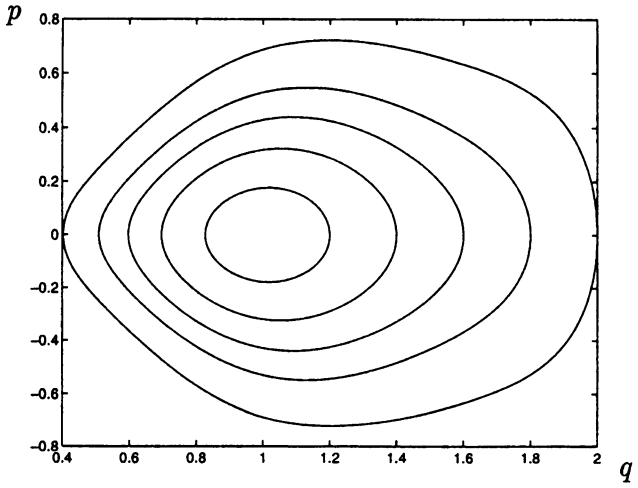

FIG. 2. Phase portrait for the unforced undamped system, for $P_0 = 0, \overline{\alpha} = 0$, and $\Delta = 1$ with equilibrium at $(q,p) = (1,0)$

For determining the equilibrium points in the case $P_0 \neq 0$, it follows from (46) and (47) that we must have $p = 0$ and $V'(q;\Delta) = 0$. Using (38) and (45), we find that the latter condition is equivalent to determining the roots of

$$\bar{g}(q;\Delta) - P_0 = 0. \tag{48}$$

Clearly, if $\bar{g}(\cdot;\Delta)$ is not monotone as in the case $\Delta = 1$ of Fig. 1, then for some choices of P_0 there will be multiple roots of (48). However, in those cases where $\bar{g}(\cdot;\Delta)$ is a strictly decreasing function, a mere shift of the equilibrium point along the q-axis will be the only effect of changing P_0. The value of Δ below which $\bar{g}(\cdot;\Delta)$ ceases to be monotone is approximately $\Delta = 9.59$.

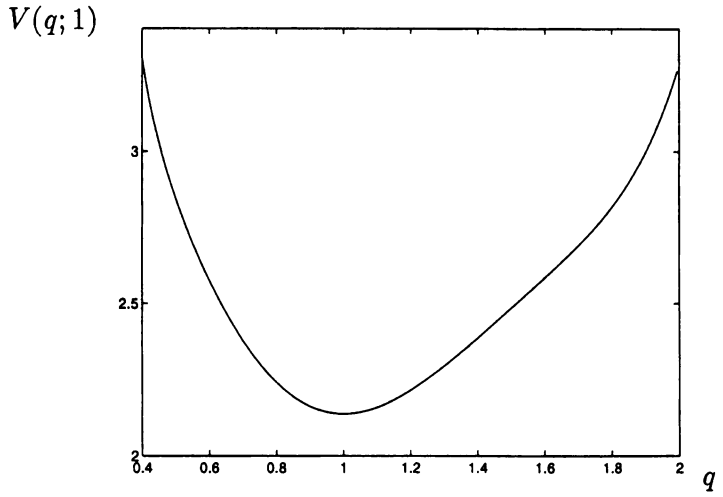

FIG. 3. Cross section of the Hamiltonian; $H = H(q,0) = V(q;1)$ for $P_0 = 0$ and $\overline{\alpha} = 0$

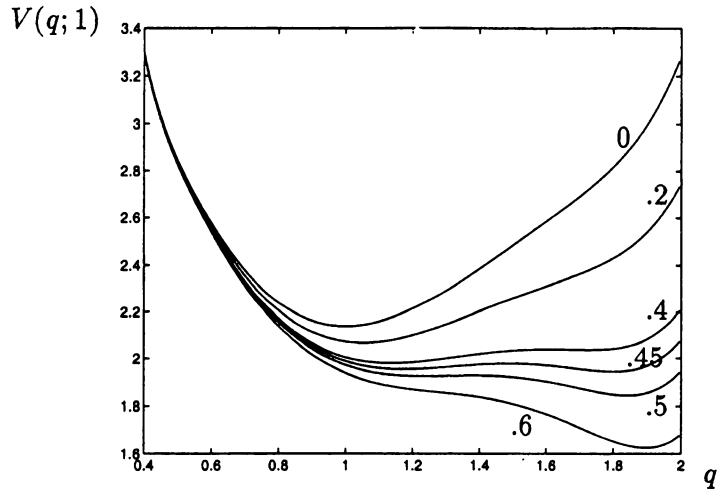

FIG. 4. The effect of an increase of P_0 on the Hamiltonian. Cross section $H = H(q,0) = V(q;1)$ for $\overline{\alpha} = 0$, and values of P_0 as indicated

Now, let us suppose that $\overline{g}(\cdot;\Delta)$ is nonmonotone, and for the sake of example take $\Delta = 1$ (any $\Delta < 9.59$ is qualitatively similar). In this case, as the static pressure P_0 is increased from zero the cross section of $H = H(q,p)$ at $p = 0$ undergoes a series of changes as illustrated in Fig. 4 for $\overline{\alpha} = 0$. If we let q^* denote any equilibrium point of the system, i.e., a value of q at which $V'(q;1) = 0$, we see that q^* will depend on P_0 as shown in Fig. 5. For values of P_0 between $P_{c1} = .39$ and $P_{c2} = .51$ there are three equilibria and the phase portrait becomes similar to Fig. 6. The corresponding Hamiltonian $H = H(q,p)$ is said to represent a double-well potential. In this case, two of the equilibrium points are stable

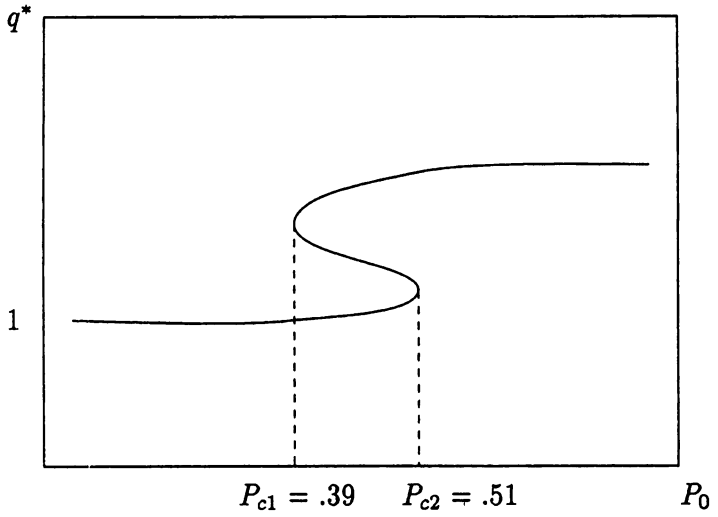

FIG. 5. Schematic bifurcation diagram for the equilibrium points: $\overline{\alpha} = 0$ and $\Delta = 1$

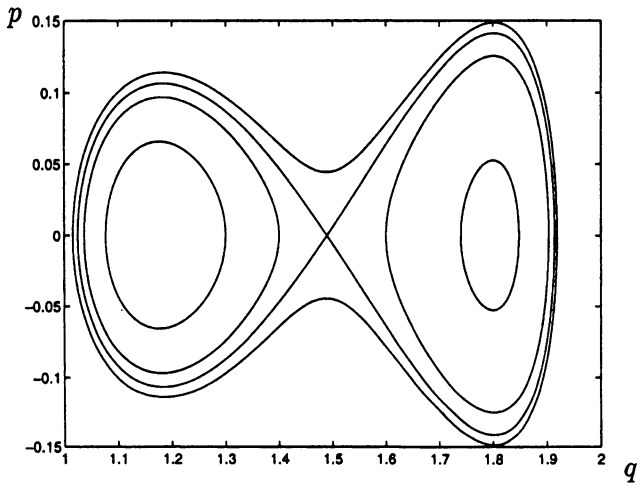

FIG. 6. Phase portrait for the unforced undamped system for $P_0 = .45, \overline{\alpha} = 0$,and $\Delta = 1$

since they correspond to local minima of the potential $V(q;1)$. The eigenvalues of the Hessian of $H(q,p)$ at these two points are purely imaginary, and the points are known as elliptic. The Hessian of $H(q,p)$ at the equilibrium point that lies between these two has two real eigenvalues of opposite sign and such an equilibrium point is known as a saddle. Associated with the saddle point (q_s, p_s), say, are two orbits on which $H = H(q(t), p(t))$ is constant. On both of these orbits $(q(t), p(t)) \to (q_s, p_s)$ as $t \to +\infty$ and as $t \to -\infty$, and they are known [12] as homoclinic orbits.

The microstructural coefficient $\overline{\alpha}$ in (37) gives rise to a dynamical potential that has no effect on the position of the equilibrium points since p vanishes at these places. However,

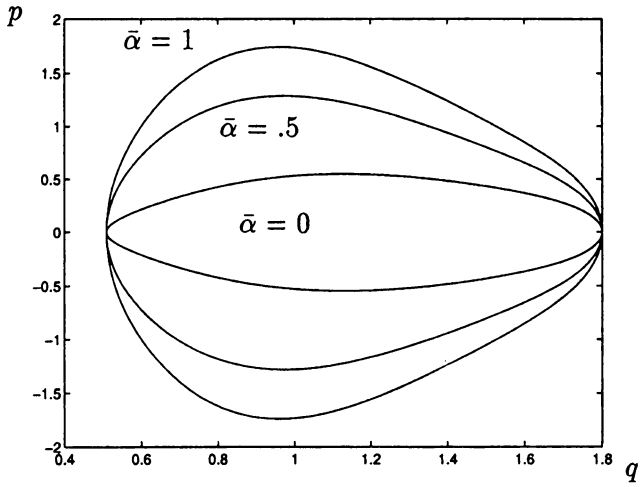

FIG. 7. Periodic orbits of equal energy for $P_0 = 0, \Delta = 1$, and different values of $\bar{\alpha}$

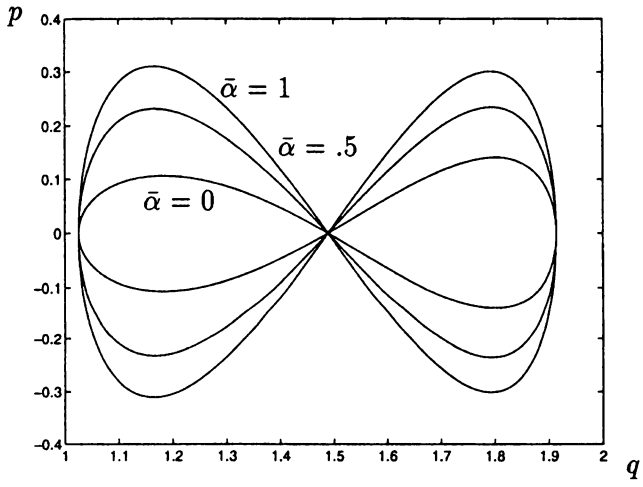

FIG. 8. Homoclinic orbits of equal energy for $P_0 = .45, \Delta = 1$, and different values of $\bar{\alpha}$

it does affect the maximum and minimum values of the generalized momentum p on any level curve $H(q,p) = const.$ without altering the maximum and minimum values of the generalized coordinate q. Figure 7 shows a set of level curves $H(q,p) = const.$ for different values of $\bar{\alpha}$, and for $P_0 = 0$, when the Hamiltonian represents a single-well potential. The level curves correspond to the same constant value of $H(q,p)$, and they all intersect at the points $(q,p) = (1.8, 0)$, and $(q,p) = (.51, 0)$. However, for the different values of $\bar{\alpha}$ the generalized momentum p has different amplitudes. Thus, in terms of a motion, $\bar{\alpha}$ changes the maximum value of the generalized momentum on a trajectory *without* changing its amplitude.

The extreme values of the generalized momentum for a motion along a periodic orbit as well as along the homoclinic orbit of a double-well potential are affected in the same way. This is shown, in the case of homoclinic orbits, in Fig. 8.

6. Forced oscillations in the presence of viscosity. We turn now to the behavior of (34) for the case $0 < \varepsilon \ll 1$, when the external forcing (33) and the viscosity are small. Thus, in terms of the variables q and p of (40) and (42) and the auxiliary functions defined in (43) and (45), the governing equation of motion (34) may be written as the system

$$\dot{q} = \frac{p}{Q(q)}, \tag{49}$$

$$\dot{p} = \frac{p^2 Q'(q)}{2Q(q)^2} - V'(q;\Delta) - \varepsilon\bar{\mu}\frac{4\Delta pq}{(q^3+\Delta)} + q^2\varepsilon f\sin(\omega t). \tag{50}$$

Clearly, (49) is the same as (46) while (50) corresponds to (47) with the addition of the viscosity and forcing terms. This system has the general form

$$\dot{\mathbf{u}} = \mathbf{h}(\mathbf{u}) + \varepsilon\mathbf{k}(\mathbf{u},t), \tag{51}$$

where $\mathbf{u} = (q,p)$, and $\mathbf{h}(\mathbf{u})$ and $\mathbf{k}(\mathbf{u},t)$ are obvious from (49) and (50), and its study is facilitated by the use of the *Poincaré map.* (See, e.g., [12], [4].)

6.1. *The Poincaré map.* Let $\mathbf{u}(t) = \varphi_t(\mathbf{u}_0, t_0)$ denote the solution of (51) that passes through $\mathbf{u}_0$ at time t_0. Then, if T is the period of the forcing function $\varepsilon\mathbf{k}(\mathbf{u},\cdot)$, the Poincaré map $\mathcal{P} : \mathbb{R}^2 \to \mathbb{R}^2$ is defined by

$$\mathcal{P}(\mathbf{u}) = \varphi_{t_0+T}(\mathbf{u}, t_0), \tag{52}$$

which indicates where the solution takes a generic pair $\mathbf{u}(q,p)$ after T units of time. This is similar to a stroboscopic image that would be obtained if the period of the stroboscope was T. Under the action of the Poincaré map the periodic orbits of (51) with period T will appear as fixed points. Periodic orbits of period nT will appear as fixed points for the map $\mathcal{P}^n$, i.e., $\mathcal{P}$ applied n consecutive times.

A periodic orbit of (51) is stable if the corresponding fixed points of the Poincaré map $\mathcal{P}(\mathbf{u})$ are stable. Thus, if a fixed point of the nth iterate $\mathcal{P}^n(\mathbf{u})$ is stable then the associated periodic orbit of (51) is stable, and small initial perturbations from the orbit will remain small for all time. If (51) has an equilibrium saddle point then the Poincaré map will have an equilibrium saddle point, which means that the gradient of the Poincaré map at the equilibrium point has two real eigenvalues, one of which is less than 1 in modulus and the other of which has modulus greater than 1. Sufficiently near the saddle point of the Poincaré map the eigenvectors corresponding to these eigenvalues define the tangential directions of the so-called one-dimensional stable and unstable *invariant manifolds* of the Poincaré map. For the unforced and undamped system as illustrated in Fig. 6, the homoclinic orbits are equivalent to the invariant manifolds of the Poincaré map corresponding to the equilibrium saddle point. In this case, the stable and unstable manifolds coincide. However, such homoclinic orbits are expected to become distinct and possibly even entangled when the system is either damped or subject to some external

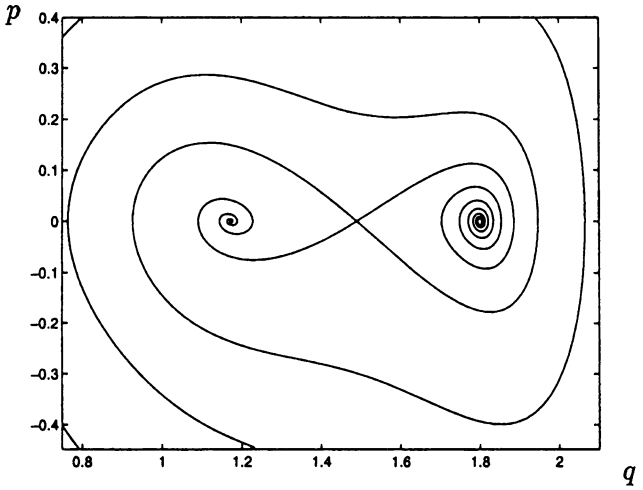

FIG. 9. Equilibrium points $(1.17, 0), (1.49, 0)$, and $(1.8, 0)$ of (49), (50) and their basins of attraction for $\overline{\alpha} = 0, P_0 = .45, \overline{\mu} = .5, \Delta = 1$, and $f = 0$

forcing. Figure 9 shows an example of distinct one-dimensional stable and unstable manifolds when the system is damped.

6.2. *The case* $f = 0, \overline{\mu} > 0$. When $f = 0$ so that there is no external time periodic forcing on the system, then any initial disturbance will eventually die out and the motion will come to rest at an equilibrium point if $\overline{\mu} > 0$. For $P_0 < P_{c1}$ or $P_0 > P_{c2}$ there is only one stable equilibrium point, and for $P_{c2} > P_0 > P_{c1}$ there are two, and the one to which the motion is attracted will depend on the initial conditions. Figure 9 shows the basins of attraction for the two stable equilibria in the case that $P_0 = .45, \overline{\alpha} = 0$, and $\varepsilon\overline{\mu} = .5$. The curve that divides these basins corresponds to the one-dimensional stable manifold of the Poincaré map for the saddle point. The one-dimensional unstable manifolds connect to the saddle point and end at the two respective stable equilibria.

6.3. *The case* $f > 0, \overline{\mu} > 0$. In the presence of both viscosity and a harmonic forcing with $\varepsilon \ll 1$, the situation is somewhat similar; instead of fixed equilibrium points, however, there are small periodic orbits in the neighborhood of the original fixed points, both in the case of the single- as well as the double-well potential. These orbits have the same stability characteristics as the corresponding fixed points had in the case that $f = 0$. It may be noted that these orbits are the trajectories for the motion that would be predicted as a result of a linearization of the system about each fixed point. In general, however, these are not the only periodic orbits present, since some of the original periodic trajectories for the motion of the undamped and unforced Hamiltonian system (46), (47) may, under small external forcing and small viscosity, retain their orbital character. Such orbits will be referred to as preserved orbits or resonant orbits. In addition, totally new orbits may be created through various types of bifurcations (such as saddle node bifurcations, or period doublings), as one or more of the system parameters $f, \overline{\mu}, \overline{\alpha}$, or P_0 is varied (see [12]).

If one admits only small amplitude motions and linearizes the system (49), (50) about the equilibrium points then much of the interesting nonlinear character of orbits, inherent in the original system, is lost. This approach would severely limit the scope of possible applications that could take full account of the nonlinear characteristics of this system. Moreover, even if a motion eventually settles to one of small amplitude that may be described adequately by a linearization of the system, such a linearization cannot be expected to give an indication of the type of transients that might have occurred. In this context, chaotic transients are of special importance since they can give rise to high amplitude and unpredictable motions. Mainly, a motion of this type exhibits transients that have sensitive dependence on initial conditions, but it eventually settles into a periodic or quasi-periodic state.

6.3.1. *The case of the single-well potential.* Identifying all the subharmonic orbits that may occur in a nonlinear system is in general a difficult task. It requires a detailed study of the steady state behavior of the system for various initial conditions as a function of the parameters of the system. However, for a system that is a perturbation of an integrable Hamiltonian system, such as (49) and (50), the preserved orbits mentioned above are relatively easy to characterize. These orbits are close to the unperturbed constant energy orbits and have periods given by

$$\mathcal{T} = \frac{m}{n}T,$$

where T is the period of the time periodic forcing and m and n are integers. The existence of such orbits can be determined by the use of Melnikov's method [12], [14]. Thus, consider a system of the form (51) where $\mathbf{k}(\mathbf{u}, \cdot)$ has period T, which is Hamiltonian with an elliptic equilibrium point surrounded by elliptic orbits when $\varepsilon = 0$. In the case that $0 < \varepsilon \ll 1$, there exists a subharmonic motion on an orbit of period $\mathcal{T} = \frac{mT}{n}$, where m and n are relatively prime integers, if the subharmonic Melnikov function has simple zeros. This function is defined by

$$M^s(\lambda) = \varepsilon \int_0^{\frac{mT}{n}} \mathbf{h}(\mathbf{u}^*(t)) \wedge \mathbf{k}(\mathbf{u}^*(t), t + \lambda)\, dt, \tag{53}$$

where $\mathbf{h} \wedge \mathbf{k} = h_1 k_2 - h_2 k_1$ and where $\mathbf{u}^*(t)$ denotes the trajectory of a periodic motion on an orbit of the unperturbed system that has period $\frac{mT}{n}$. Comparing (49) and (50) with (51) we see that in the present problem the subharmonic Melnikov function has the form

$$M^s(\lambda) = \varepsilon \int_0^{\frac{mT}{n}} \frac{p^*(t)}{Q(q^*(t))} \left(-\frac{4\bar{\mu}\Delta p^*(t) q^*(t)}{([q^*(t)]^3 + \Delta)} + [q^*(t)]^2 f \sin(\omega(t + \lambda)) \right) dt, \tag{54}$$

where $(q^*, p^*)(t)$ is the trajectory of a motion on an orbit of (46), (47) having period $\frac{mT}{n}$. Of course, here $T = \frac{2\pi}{\omega}$.

After some algebraic simplifications we find that the condition for $M^s(\lambda) = 0$ to have simple roots has the form

$$\frac{f}{\bar{\mu}} \geq \frac{\Psi^s}{\Phi^s}, \tag{55}$$

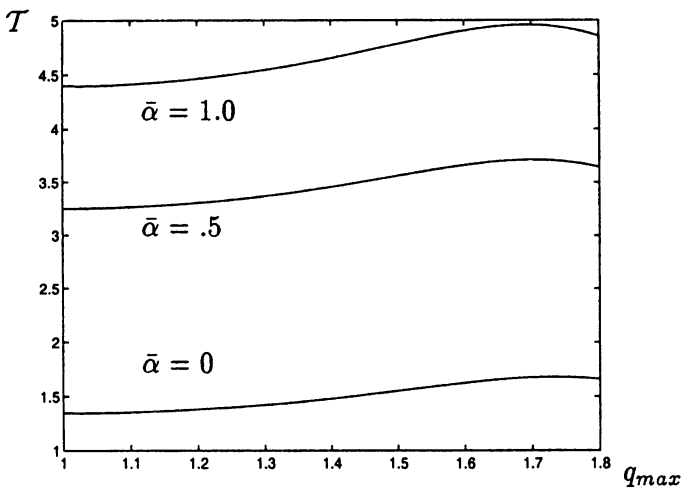

FIG. 10. The period $\mathcal{T}$ of constant-energy orbits of (46), (47) as a function of the maximum amplitude $q_{\max}$ for various values of $\bar{\alpha}$, with $P_0 = 0$ and $\Delta = 1$

where

$$\Psi^s = \int_0^{\frac{mT}{n}} \frac{4\Delta[p^*(t)]^2}{Q[q^*(t)]([q^*(t)]^3 + \Delta)} dt, \tag{56}$$

and

$$\Phi^s = \int_0^{\frac{mT}{n}} \frac{[q^*(t)]^2 p^*(t) \sin(\omega t)}{Q(q^*(t))} dt. \tag{57}$$

In order to carry out the calculations described above it is necessary to determine $(q^*, p^*)(t)$ corresponding to the given period $\frac{mT}{n}$ for the system (46), (47). We do this in the following way: First, given $\bar{\alpha}$ and Δ we find the period $\mathcal{T}$ for a motion of the system (46), (47) as a function of the maximum amplitude $q_{\max}$, as in Fig. 10. Then, with this functional relation established, we set $\mathcal{T} = \frac{mT}{n}$, determine the corresponding $q_{\max}$, and then integrate the system (46), (47) subject to the initial condition $(q(0), p(0)) = (q_{\max}, 0)$. This gives $(q^*, p^*)(t)$, and then (56) and (57) can be used to construct the bound (55) on $\frac{f}{\mu}$, above which the Melnikov function has zeros.

Now, to determine $\mathcal{T}(q_{\max})$ so that Fig. 10 can be constructed, we first recall from (44) that

$$p^2 = 2Q(q)(H(q,p) - V(q;\Delta)). \tag{58}$$

Then, from (46) we may write

$$\dot{q} = \pm\sqrt{\frac{H(q(t),p(t)) - V(q(t);\Delta)}{2Q(q(t))}}. \tag{59}$$

But on the trajectory of such a motion we have

$$H(q(t),p(t)) = H(q(0),p(0)) = H(q_{\max},0) = V(q_{\max};\Delta), \tag{60}$$

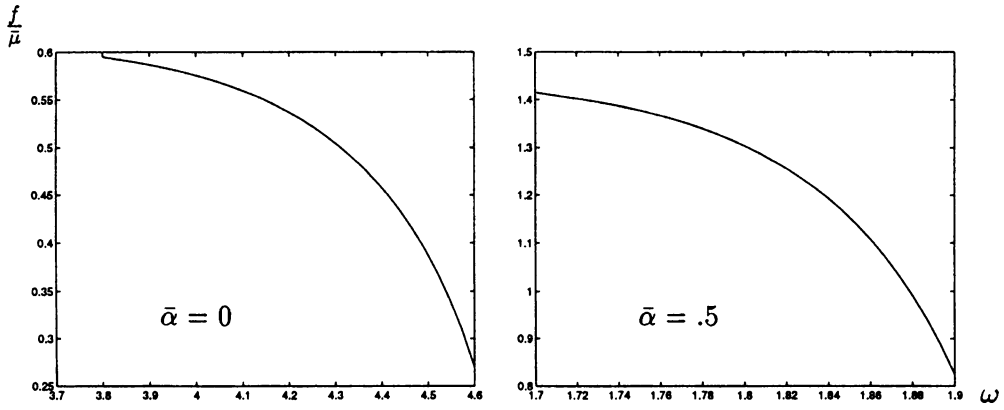

FIG. 11. Melnikov boundaries for preserved periodic orbits with $m = n = 1$ in the case of the single-well potential, for $\overline{\alpha} = 0$ and $\overline{\alpha} = .5$. Here, $P_0 = 0$ and $\Delta = 1$.

so that

$$dt = \pm\sqrt{\frac{2Q(q(t))}{V(q_{\max};\Delta) - V(q;\Delta)}}dq. \tag{61}$$

Finally, since the motion on a trajectory requires $H(q_{\max}, 0) = H(q_{\min}, 0) = V(q_{\min};\Delta)$, we can determine $q_{\min}$ in terms of $q_{\max}$ and conclude that

$$\mathcal{T}(q_{\max}) = 2\int_{q_{\min}}^{q_{\max}} \sqrt{\frac{2Q(q)}{V(q_{\max},\Delta) - V(q;\Delta)}}dq. \tag{62}$$

Figure 10 shows $\mathcal{T}(q_{\max})$ for the unperturbed conservative system (46), (47). From here we see that the period of an orbit with a fixed maximum amplitude $q_{\max}$ is an increasing function of $\overline{\alpha}$. Notice also that for the values of $\overline{\alpha}$ shown, the period initially increases with $q_{\max}$ but then decreases after approximately $q_{\max} = 1.7$.

In Fig. 11 we show $\frac{f}{\mu}$ vrs. ω $(= \frac{2\pi}{T})$ for $\overline{\alpha} = 0$ and $\overline{\alpha} = .5$; these graphs represent the equality condition in (55) for $m = n = 1$. For a fixed forcing frequency ω, the ratio $\frac{f}{\mu}$ must be sufficiently large to lie on or above this graph before the perturbed system can support a motion on a preserved periodic orbit that has the same period ($m = n = 1$) as that of the motion for the unperturbed Hamiltonian system about its equilibrium point.

6.3.2. *The case of the double-well potential.* As has been mentioned earlier in relation to Fig. 5, the phase portrait of the unperturbed system changes its appearance completely as the static pressure P_0 is increased beyond $P_{c1} = .39$ because of the criterion of a saddle point and a new elliptic point (see Fig. 6). Now we consider this case where P_0 is such that the unperturbed Hamiltonian system has a double-well potential.

Subharmonic orbits. As in the case of the single-well potential, subharmonic orbits of the system (49), (50) may be created through the preservation of the periodic orbits of the unperturbed system. Melnikov's method for subharmonic orbits can be used also in the case of the double-well potential to determine the existence of preserved orbits after perturbation. Figure 12 shows, for each forcing frequency ω, the thresholds of $\frac{f}{\mu}$ above

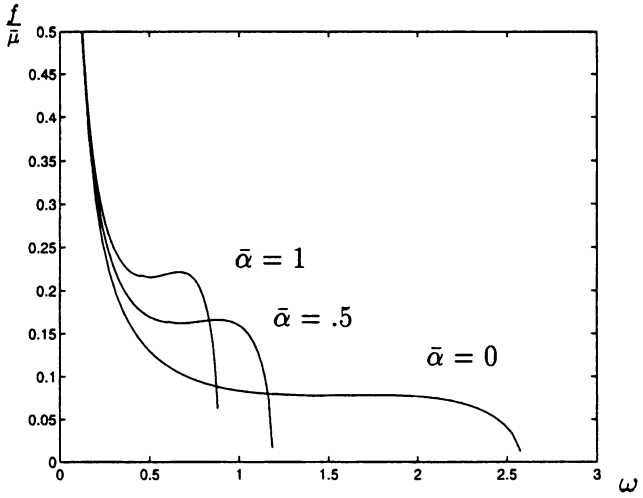

FIG. 12. Melnikov boundaries for preserved periodic orbits inside the left homoclinic orbit of Fig. 6 with $m = n = 1$ and for various values of $\bar{\alpha}$. Here, $P_0 = .45$ and $\Delta = 1$.

which the orbits of the same frequency that are inside of the homoclinic orbit on the left side of the saddle point in Fig. 6 are preserved. It is worth emphasizing that the graphs in Fig. 12 correspond to the lowest values of $\frac{f}{\overline{\mu}}$ for the creation of preserved orbits. There is no guarantee of the existence of these orbits for all values of $\frac{f}{\overline{\mu}}$ larger than the ones indicated in this figure because the subharmonic orbits thus created may go through other types of bifurcations such as period doubling. From Fig. 12, we may conclude that as the material parameter $\overline{\alpha}$ is increased from zero, there is a corresponding increase in the critical ratio $\frac{f}{\overline{\mu}}$ at which orbits are preserved having the same frequency ($m = n = 1$) as the forcing frequency ω. Also, we note from Fig. 12 that for a given value of $\overline{\alpha}$ there is a corresponding critical forcing frequency ω above which there are no preserved orbits that have the same frequency for any $\frac{f}{\overline{\mu}}$; for $\overline{\alpha} = 1$ the critical frequency is approximately $\omega = .9$.

Homoclinic orbits and chaotic motion. In Sec. 6.2 we gave an example that showed one way in which the homoclinic orbits corresponding to the saddle point can be broken. In that case the invariant manifolds of the Poincaré map are connected (tangentially) only at the saddle point after breaking up. Depending upon the values of the forcing amplitude εf, the viscosity $\varepsilon\overline{\mu}$, and the forcing frequency ω, the invariant manifolds of the Poincaré map may have (non-tangential) transversal intersections. Any such intersection implies the existence of an infinite number of intersections since a point at the intersection, which is on both the stable and the unstable manifolds, must be mapped through the repeated Poincaré map to another point on both the stable and the unstable manifolds. Such intersections of the invariant manifolds of the Poincaré map are known as homoclinic points. The creation of such points as a result of a change in the parameters of the system is referred to as a homoclinic bifurcation. In the same way that the equilibrium point of the Poincaré map represents a periodic orbit of the continuous time system, homoclinic

points of the Poincaré map represent trajectories that either converge to the saddle orbit of the continuous time system or diverge from it as $t \to \infty$ or as $t \to -\infty$. These types of trajectories that correspond to the existence of homoclinic points are necessary for chaotic motion. Perhaps of more significance, however, is that such trajectories may result in chaotic transients eventually leading to periodic or quasi-periodic motion. Though such transients may seem harmless at first sight because they eventually are tame, on the other hand a trajectory of this kind may cross a critical boundary or a constraint restriction of a physical nature at some time that could be undesirable. For example, the amplitude of an allowable motion may be restricted because of design considerations.

The existence of homoclinic points may be determined by the use of another version of Melnikov's method. Thus, consider a system of the form (51) where $\mathbf{k}(\mathbf{u}, \cdot)$ has period T, and $0 \leq \varepsilon \ll 1$. We assume that when $\varepsilon = 0$ the unperturbed system has a homoclinic orbit associated with a saddle point so that the phase portrait is as in Fig. 6. A sufficient condition for the perturbed system to possess homoclinic points is that the homoclinic Melnikov function $M^h(\lambda)$ must have simple zeros. This function is defined [12] by

$$M^h(\lambda) = \varepsilon \int_{-\infty}^{\infty} \mathbf{h}(\mathbf{u}^0(t)) \wedge \mathbf{k}(\mathbf{u}^0(t), t + \lambda) dt, \tag{63}$$

where $\mathbf{u}^0(t)$ is the trajectory of a motion on the unperturbed homoclinic orbit; thus if $\mathbf{u}_s$ is the saddle point then $\mathbf{u}^0(t) \to \mathbf{u}_s$ as $t \to \infty$ or as $t \to -\infty$.

Comparing (51) with (49) and (50), we find that in the present case

$$M^h(\lambda) = \varepsilon \int_{-\infty}^{\infty} \frac{p^0(t)}{Q(q^0(t))} \left(-\overline{\mu} \frac{4\Delta p^0(t) q^0(t)}{[q^0(t)]^3 + \Delta} + [q^0(T)]^2 f \sin(\omega(t + \lambda)) \right) dt, \tag{64}$$

where $(q^0, p^0)(t)$ is the trajectory of a motion on one of the homoclinic orbits of (46), (47). Denoting the maximum amplitude of $q^0(t)$ on the right-hand side homoclinic orbit in Fig. 6 by $q_{\max}$ and the minimum amplitude of $q^0(t)$ on the left-hand side homoclinic orbit by $q_{\min}$, the initial data for the right-hand side homoclinic orbit is $(q^0, p^0)(0) = (q_{\max}, 0)$, and the initial data for the left-hand side homoclinic orbit is $(q^0, p^0)(0) = (q_{\min}, 0)$. As in the case earlier for the subharmonic orbits, the condition for $M^h(\lambda)$ to have simple zeros can be expressed in the form

$$\frac{f}{\overline{\mu}} \geq \frac{\Psi^h}{\Phi^h}, \tag{65}$$

where

$$\Psi^h = \int_{-\infty}^{\infty} \frac{4\Delta [p^0(t)]^2}{Q(q(t)) q^0(t) [q^0(t)]^3 + \Delta} dt \tag{66}$$

and

$$\Phi^h = \int_{-\infty}^{\infty} \frac{[q^0(t)]^2 p^0(t) \sin(\omega t)}{Q(q(t))} dt. \tag{67}$$

Since analytical expressions for the unperturbed homoclinic orbits are not available, the integration above must be done numerically. The results are summarized in Figs. 13 and 14. Figure 13 (see p. 240) shows the ratio $\frac{f}{\overline{\mu}}$ for which homoclinic points are

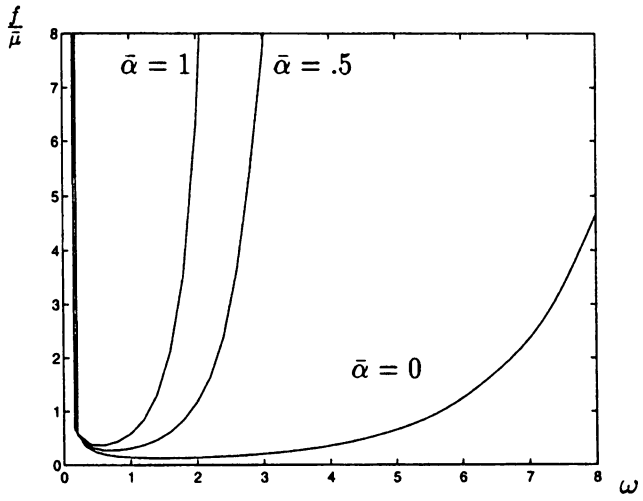

FIG. 13. Lower boundaries of $\frac{f}{\bar{\mu}}$ vrs. the forcing frequency ω for the existence of homoclinic orbits of the forced and damped system; the left-side homoclinic orbit from Fig. 6. Here, $P_0 = .45$ and $\Delta = 1$.

created as a function of the forcing frequency $\omega = \frac{2\pi}{T}$, for different values of $\bar{\alpha}$, and corresponding to the left-hand side homoclinic orbit of the unperturbed system as shown in Fig. 6. Figure 14 shows the corresponding ratio $\frac{f}{\bar{\mu}}$ for the right-hand side homoclinic orbit from Fig. 6. According to (65), the curves the Figs. 13 and 14 represent the lowest value of the ratio $\frac{f}{\bar{\mu}}$ above which there will be transversal intersections of the invariant stable and unstable manifolds of the Poincaré map: Fig. 13 corresponds to the left half of the phase portrait from the saddle point, and Fig. 14 corresponds to the right half. Clearly it is possible that the invariant manifolds corresponding to the right-hand side of the saddle point have intersections for a given $\frac{f}{\bar{\mu}}$ and $\bar{\alpha}$ while the ones on the left-hand side do not. For example for $\bar{\alpha} = 0$ and $\omega = 1$ the threshold for the creation of homoclinic orbits is $\frac{f}{\bar{\mu}} \approx .1$ for the left-side homoclinic orbit, and $\frac{f}{\bar{\mu}} \approx .05$ for the right-side homoclinic orbit. Thus, for $\varepsilon f = 0.01$ and $\varepsilon\bar{\mu} = 0.01$ there are homoclinic points on the invariant manifolds of the Poincaré map corresponding to both sides of the saddle point. Figure 15 shows the invariant manifolds of the Poincaré map for this situation. In this case, the initial condition $(q(0), p(0)) = (1.4, -0.1)$ leads to the trajectory as shown in Fig. 16 (see p. 242). Note that the motion corresponding to this trajectory exhibits large-amplitude transients before becoming periodic in the neighborhood of an equilibrium point. In contrast to this, Fig. 17 (see p. 242) shows the transient trajectory from the same initial condition to a similar periodic orbit in the absence of homoclinic orbits. In this case, $\varepsilon f = 0.01$ and $\varepsilon\bar{\mu} = 0.25$, so that $\frac{f}{\bar{\mu}}$ is 96% smaller and the influence of viscosity is fairly strong. In general, from Figs. 13 and 14 we see that for a given forcing frequency ω, the critical value of $\frac{f}{\bar{\mu}}$ for the existence of homoclinic points can be made larger by increasing the material parameter $\bar{\alpha}$. In particular, for fixed ω and $\frac{f}{\bar{\mu}}$ the system will not experience chaotic transients if $\bar{\alpha}$ is sufficiently large.

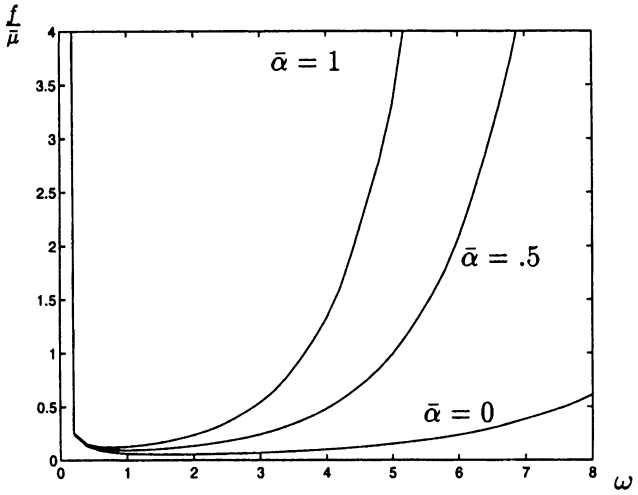

FIG. 14. Lower boundaries of $\frac{f}{\bar{\mu}}$ vrs. the forcing frequency ω for the existence of homoclinic orbits of the forced and damped system; the right-side homoclinic orbit from Fig. 6. Here, $P_0 = .45$ and $\Delta = 1$.

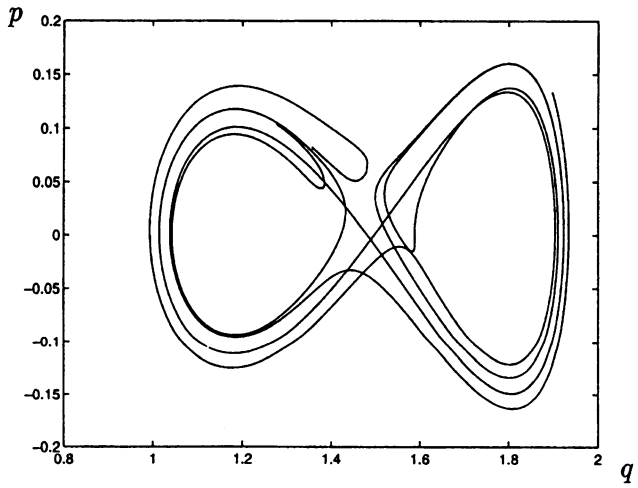

FIG. 15. Invariant manifolds of the Poincaré map corresponding to the saddle point of Fig. 6. Here, $P_0 = .45, \overline{\alpha} = 0, \varepsilon f = 0.01, \varepsilon\overline{\mu} = 0.01, \omega = 1$, and $\Delta = 1$.

Recall that for values of $\frac{f}{\bar{\mu}}$ larger than those graphed in Fig. 12 there is no guarantee that stable preserved subharmonic orbits will indeed be possible for the perturbed system. There is the possibility that other types of bifurcations could occur such as period doubling. All of these can change the complete character of the motion. This is illustrated in the purely chaotic trajectory of Fig. 18 (see p. 243) for which we have considered a ratio $\frac{f}{\bar{\mu}} = 2$ for $\omega = 1$ and $\overline{\alpha} = 0$.

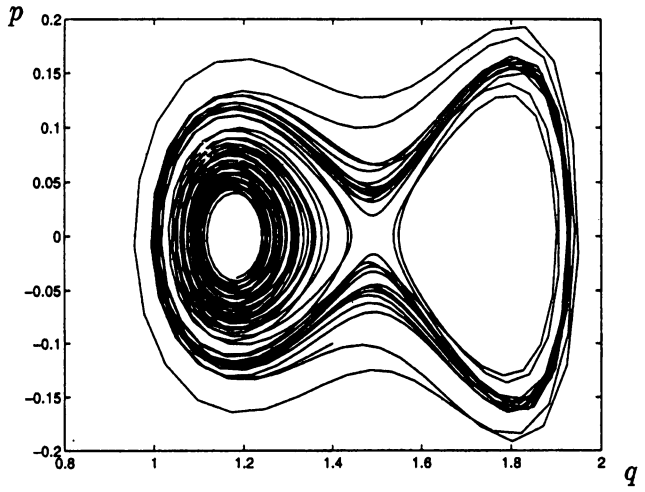

FIG. 16. Transient trajectory to small periodic oscillations about an equilibrium point with initial condition $(q(0), p(0)) = (1.4, -1)$. Here, $P_0 = .45, \overline{\alpha} = 0, \varepsilon f = 0.01, \varepsilon\overline{\mu} = .01, \omega = 1$, and $\Delta = 1$.

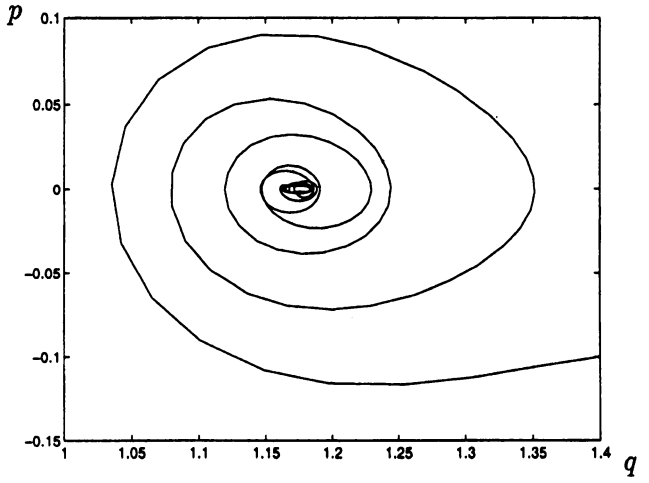

FIG. 17. Transient trajectory to small periodic oscillations about an equilibrium point with initial condition $(q(0), p(0)) = (1.4, -.1)$. Here, $P_0 = .45, \overline{\alpha} = 0, \varepsilon f = .01, \varepsilon\overline{\mu} = .25, \omega = 1$, and $\Delta = 1$.

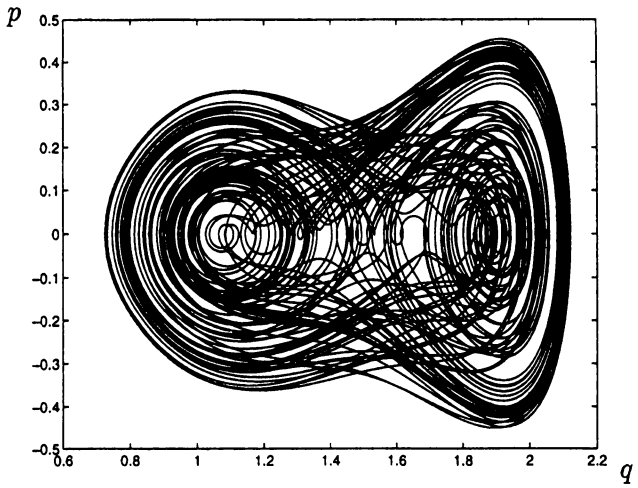

FIG. 18. Chaotic orbit with initial condition $(q(0), p(0)) = (1.4, -.1)$ for $P_0 = .45, \overline{\alpha} = 0, \varepsilon f = .2$, $\varepsilon\overline{\mu} = .1, \omega = 1$, and $\Delta = 1$.

7. Concluding remarks. We assumed that a spherical shell is made of such material that it can have two relatively stable stages of equilibrium for the same internal pressure. Dynamically, the material is viscoelastic and the shell can undergo a phase transition during its motion wherein it moves between the two energy wells that contain the respective equilibrium states. During the process of phase transition the resulting Hamiltonian system corresponds to that of a double-well potential. Though even in this case small periodic orbits about a stable equilibrium point are possible, the existence of a saddle point for the unperturbed system and two stable equilibrium points makes the dynamics more complicated. One of the main conclusions of this work is that large-amplitude transients are possible before the system reaches a state of small oscillations about one of the fixed points. Another, is that within each of the two potential wells the possible periodic motions are distinct. Further, we found how the period of free oscillations and the amplitude of the generalized momenta depend on the microstructural coefficient $\overline{\alpha}$. Perhaps our observations and predictions can give some guidance to a dynamical experimental program that is aimed at characterizing the material properties of shape memory alloys.

It is known that multi-well energy potentials can be used to predict many of the features of the finely twinned microstructures that are observed in statically loaded crystals [3]. The possibility of chaotic behavior, as shown in the present work, is a dynamical manifestation of the nonconvex multi-well energy potential and, thus, may be interpreted as a dynamical counterpart of the finely twinned mixtures and coexistent phase structures that arise in the static situation.

Acknowledgment. The National Science Foundation and Alliant Techsystems Inc. are gratefully acknowledged for their partial support of this work. In addition, Y. K. and

J. H. Y. wish to thank the Department of Aerospace Engineering and Mechanics at the University of Minnesota for the use of its facilities.

REFERENCES

[1] R. Abeyaratne and J. K. Knowles, *Dynamics of propagating phase boundaries: Thermoelastic solids with heat conduction*, Archive for Rational Mechanics and Analysis **126**(3), 203–230 (1994)

[2] M. Baker and J. L. Ericksen, *Inequalities restricting the form of the stress-deformation relations for isotropic elastic solids and Reiner-Rivlin fluids*, J. Wash. Acad. Sci. **44**, 33–35 (1954)

[3] C. Chu and R. D. James, *Biaxial loading experiments on Cu-Al-Ni single crystals*, AMD-Vol. 181, ASME, 61–69 (1993)

[4] Thomas S. Parker and Leon O. Chua, *Chaos: A tutorial for engineers*, Proceedings of the IEEE **75**(8), 982–1008 (1987)

[5] P. M. Culkowski and H. Reismann, *The spherical sandwich shell under axisymmetric static and dynamic loading*, Journal of Sound and Vibration **14**, 229–240 (1971)

[6] J. E. Dunn and R. L. Fosdick, *Thermodynamics, stability, and boundedness of fluids of complexity 2 and fluids of second grade*, Archive for Rational Mechanics and Analysis **56**(3), 191–252 (1974)

[7] F. Falk, *Model free energy, mechanics, and thermodynamics of shape memory alloys*, Acta Metallurgica **28**, 1773–1780 (1980)

[8] R. L. Fosdick and G. P. MacSithigh, *Minimization in incompressible nonlinear elastic theory*, Journal of Elasticity **16**, 267–301 (1986)

[9] R. L. Fosdick, W. H. Warner, and J. H. Yu, *Steady, structured shock wave in a viscoelastic solid of differential type*, International Journal of Engineering Science **28**(6), 469–483 (1990)

[10] B. P. Gautham and N. Ganesan, *Vibration and damping characteristics of spherical shells with a viscoelastic core*, Journal of Sound and Vibration **170**(3), 289–301 (1994)

[11] H. Goldstein, *Classical Mechanics*, second edition, Addison-Wesley Publishing Company, Reading, MA, 1980

[12] J. Guckenheimer and P. Holmes, *Nonlinear oscillations, dynamical systems, and bifurcation of vector fields*, Applied Mathematical Sciences, Vol. 42, Springer-Verlag, Berlin, 1983

[13] Z. Guo and R. Solecki, *Free and forced finite-amplitude oscillations of an elastic thick-walled hollow sphere made of incompressible material*, Archiwum Mechaniki Stosowanej **3**(15), 427–433 (1963)

[14] Y. Ketema, *A physical interpretation of Melnikov's method*, International Journal of Bifurcation and Chaos **2**(1), 1–9 (1991)

[15] J. K. Knowles and M. T. Jakub, *Finite dynamic deformation of an incompressible elastic medium containing a spherical cavity*, Archive for Rational Mechanics and Analysis **18**, 367–378 (1965)

[16] P. H. Leo, T. W. Shield, and O. P. Bruno, *Transient heat transfer effects of the pseudoelastic behavior of shape-memory wires*, Acta Metall. Mater., 2477–2485 (1993)

[17] A. Okazaki, Y. Urata, and A. Tatemichi, *Damping properties of a three layered shallow spherical shell with a constrained viscoelastic layer*, Japan Society of Mechanical Engineers International Journal, Ser. I, **33**(2), 145–151 (1990)

[18] C. Truesdell and W. Noll, *The non-linear field theories of mechanics*, Handbook of Physics, III/3, Springer-Verlag, New York, 1965

[19] J. Yu, *Ph.D. Thesis: Nonlinear oscillations of viscoelastic cylindrical and spherical shells*, University of Minnesota, 1994

[20] R. L. Fosdick and J. H. Yu, *Thermodynamics, stability and nonlinear oscillations of viscoelastic solids.* Part I: *Differential type solids of second grade*, Internat. J. Non-Linear Mech. **31** (4), 495–516 (1996)